# Ionic Species in Pulse Radiolysis of Supercritical Carbon Dioxide. 2. Ab Initio Studies on the Structure and Optical Properties of $(CO_2)_n^+$, $(CO_2)_2^-$, and $CO_3^-$ Ions

**Ilya A. Shkrob***

*Chemistry Division, Argonne National Laboratory, Argonne, Illinois 60439*

*Received: June 25, 2002; In Final Form: August 12, 2002*

Gas-phase $(CO_2)^+_{2-4}$ cations and $(CO_2)_2^-$, $CO_3^-$, $CO_3^-\cdot H_2O$ and $CO_3^-\cdot CO_2$ anions have been examined using density functional theory calculations. It is shown that the lowest energy $(CO_2)_n^+$ cations are $C_{2h}$ symmetric "ladder" structures with complete delocalization of charge and spin between the monomer units. These cations absorb in the visible due to a charge resonance band that involves their lowest $^2B_u$ and $^2A_g$ states. The "ladder" structure accounts for several trends observed in the photodestruction spectra of the $(CO_2)_n^+$ cations. For the $(CO_2)_2^+$ dimer cation, the energy and the oscillator strength of the charge resonance band compare favorably with these parameters for the solvent radical cation in supercritical (sc) $CO_2$. A close similarity between the VIS spectra of the $(N_2O)_2^+$ dimer cation (in sc $CO_2$) and the solvent cation suggests that the latter has the $(CO_2)_2^+$ dimer cation as the chromophore core. It is demonstrated that optical, Raman, and magnetic resonance spectra of the carbonate radical anion, $CO_3^-$, can be consistently accounted for by a $C_{2v}$ symmetric structure with the unique O−C−O angle of ≈113° (in water) to ≈100° (in carbonate minerals). The oscillator strength of the $A\ ^2A_1 \leftarrow X\ ^2B_2$ transition in the visible correlates with this O−C−O angle. In aqueous $CO_3^-$, the trigonal distortion is due to hydrogen bonding to a single water molecule. In sc $CO_2$ (and other nonpolar liquids), the trigonal distortion is weak, and $CO_3^-$ should be a poor light absorber. This may be the reason no dissociative electron capture in sc $CO_2$ has been observed by optical spectroscopy.

## 1. Introduction

In Part 1 of this series,[1] a transient absorption−pulse radiolysis study of intrinsic ionic species in supercritical (sc) $CO_2$, the solvent radical cation, $(CO_2)_n^+$, and the solvent radical anion, $(CO_2)_n^-$, have been reported. These ions (also referred to as "holes" and "electrons")[1−5] were observed shortly (1−100 ns) after the ionization event in sc $CO_2$. Electron and proton-transfer reactions of these two solvent ions account for most of chemical transformations occurring in radiolysis of sc $CO_2$ solutions.[1−4] Therefore, their structure and optical properties are of much interest.

The solvent radical anion, $(CO_2)_n^-$, has been previously studied using time-resolved photoconductivity. [5] The electron photodetachment spectrum obtained in these conductivity experiments matches perfectly the absorption spectrum of the $(CO_2)_n^-$ anions obtained in pulse radiolysis.[1] This suggests that the absorption band of the solvent anion is due to a bound-to-continuum electron transition from a highly localized state to an extended conduction band state. By contrast, the absorption spectrum of the $(CO_2)_n^+$ cation is a bell-shaped curve with a center at 1.63 eV and an onset at 0.6−0.8 eV (Figure 1).[1−3] The integration of this band (Figure 1) yields an oscillator strength of 0.153 for the corresponding transition. Thus, this band results from a symmetry allowed bound-to-bound transition.

In previous studies from this laboratory,[2,3] Dimitrijevic et al. suggested that the 1.63 eV band shown in Figure 1 (open circles) originates through the absorption of light by the $(CO_2)_2^+$ dimer cation (whose photodestruction spectrum in the gas phase[6] is shown in Figure 1, filled circles with bars); that is, that this dimer cation constitutes the chromophore core of the solvent radical cation in sc $CO_2$. Their conclusion is further supported by our pulse radiolysis study:[1] a similar bell-shaped VIS band was observed in pulse radiolysis of $N_2O$ solutions in sc $CO_2$. This new band (see Figure 1S(a) in the Supporting Information) appears in the optical spectra concurrently with the disappearance of the 1.63 eV band of the solvent cation. Note that $N_2O$ is a linear molecule isoelectronic with $CO_2$, and the charge transfer from $(CO_2)_2^+$ to $N_2O$, with the subsequent formation

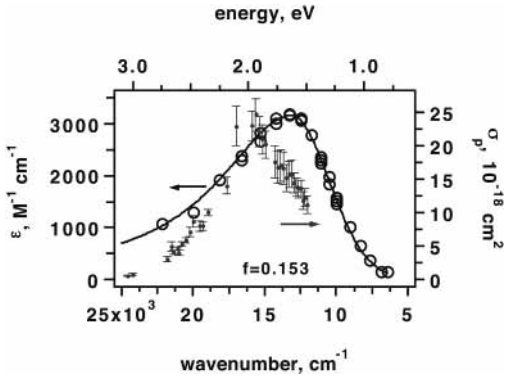


**Figure 1.** Open circles, to the left: Optical absorption spectrum of the solvent radical cation, $(CO_2)_n^+$, in radiolysed supercritical $CO_2$ ($T$ = 41 °C, $\rho$ = 837 kg/m$^3$); the data are plotted using the transient absorption results of ref 1 (open circles); $\epsilon$ is the decadic molar extinction coefficient. The line drawn through the data is a Gaussian (low-energy slope) and Lorentzian (high-energy slope) curve spliced at the center of the band. The integration yields an oscillator strength of 0.153 (for $n$ = 1.196). Filled circles, with error bars, to the right: Photodestruction cross section $\sigma_{ph}$ for the gas-phase $(CO_2)_2^+$ cluster cation as a function of the photon energy, after ref 6.

* To whom correspondence should be addressed. Phone: 630-2529516. Fax: 630-2524993. E-mail: shkrob@anl.gov.

10.1021/jp0214918 CCC: $22.00 
Published on Web 11/07/2002

of $(N_2O{\cdot}CO_2)^+$ and $(N_2O)_2^+$ cations, has been shown to occur in the gas phase.[7] Apparently, analogous charge transfer occurs in sc $CO_2$, and the resulting solute cation has similar electronic structure to that of the solvent radical cation. In this work, we argue that the visible absorption of the solvent radical cation in sc $CO_2$ results from the charge resonance $A\ ^2A_g \leftarrow X\ ^2B_u$ band of the $C_{2h}$ symmetric $(CO_2)_2^+$ dimer cation (see below). Similar charge resonance bands were also obtained for higher $C_{2h}$ symmetric $(CO_2)_n^+$ multimer cations; however, it appears that these higher "ladder" multimers do not occur in sc $CO_2$. We also discuss the possible structure of the solvent radical anion, and examine the possibility for the observation of this species in solid $CO_2$, by electron paramagnetic resonance (EPR) spectroscopy.

Pulse radiolysis studies give no evidence for the formation of $CO_3^-$,[3,4] the final product of dissociative electron attachment to $CO_2$.[8] In aqueous solutions, the carbonate radical anion exhibits a 2.05 eV band shown in Figure 1S(b).[9,10,11] This band was not observed in radiolysed sc $CO_2$,[1,4] even when the 1.63 eV band of $(CO_2)_n^+$ was eliminated by addition of "hole" scavengers. [1] Because the $CO_3^-$ anion was observed both in electron bombardment of neutral $(CO_2)_n$ clusters in the gas phase, by mass spectrometry,[8] and in $\gamma$-irradiated dry ice, by EPR spectroscopy, [12−14] a valid question is whether the $CO_3^-$ anion can exist in sc $CO_2$ and, if it does, how does it absorb? Although the carbonate radical cation has been extensively studied, both in aqueous solutions (by time-resolved optical[9−11] and Raman[15] spectroscopies) and carbonate minerals (by EPR),[16−20] no agreement exists as to why (i) this species absorbs visible light and (ii) its possible structure in solid or liquid environment. For example, it has been recently proposed that in the aqueous solution the absorbing species is a stable complex of the $CO_3^-$ anion with a carbonate anion, $CO_3^{2-}$.[11] In this work, we address both of the questions raised above. It is demonstrated that the chromophore is the $CO_3^-$ anion with reduced $C_{2v}$ symmetry. This structure accounts for the observed optical, Raman, and EPR spectra of the carbonate radical anion in various matrixes. The absorption properties strongly depend on the degree of trigonal distortion. Our calculations suggest that chemical bonding between this anion and $CO_2$ molecules in sc $CO_2$ solution is not favored energetically. It appears that $CO_3^-$ in sc $CO_2$ should be an inefficient light absorber because of weak trigonal distortion of this anion in the nonpolar environment.

To save space, background information and some data and figures are given in the Supporting Information. Sections, figures, and tables with a designator "S" after the number (e.g., Figure 1S) are placed therein.

## 2. Results and Discussion

**2.1. Solvent Radical Cation, $(CO_2)_n^+$.** A brief review of experimental[21−23] and computational[24−27] studies of the gas phase $(CO_2)_n^+$ cations is given in section 1S.1 in the Supporting Information. As explained therein, the nature of the chromophore group in such cations is not completely understood. Whereas the experimental studies[21,22,23] suggest that the staggered side-to-side structure **Ia** shown in Figure 2 is the chromophore core of all $(CO_2)_n^+$ cations, ab initio calculations by McKee and co-workers give very different structures for the dimeric and trimeric species.[24,25] To clarify the matter, we have carried out a series of calculations for $(CO_2)_n^+$ cations, including the dimer, trimer, and tetramer cations (Figures 2 and 3). Computation methods, Møller−Plesset correlation energy correction truncated at the second order (MP2) and a density functional theory (DFT) model with Becke's exchange functional and Lee−Yang−Parr correlation functional (B3LYP),[28] from the Gaussian 98 package were used.[29] The atomic orbital basis sets used in these calculations varied from the tight-binding 3-21G set to extended sets that included polarization (6-31G*) and diffuse (6-311+G*) functions. In addition, we examined several $(N_2O)_2^+$ and $(N_2O{\cdot}CO_2)^+$ cations (structures **IV** and **Va**−**Vd**, respectively) that are isoelectronic with the $(CO_2)_2^+$ dimer cation; these cations are shown in Figures 2 and 2S, respectively. Using a configuration interaction with single excitations (CIS),[29] we estimated vertical transition energies and oscillator strengths for the lower excited states of these cations. The following results were obtained:

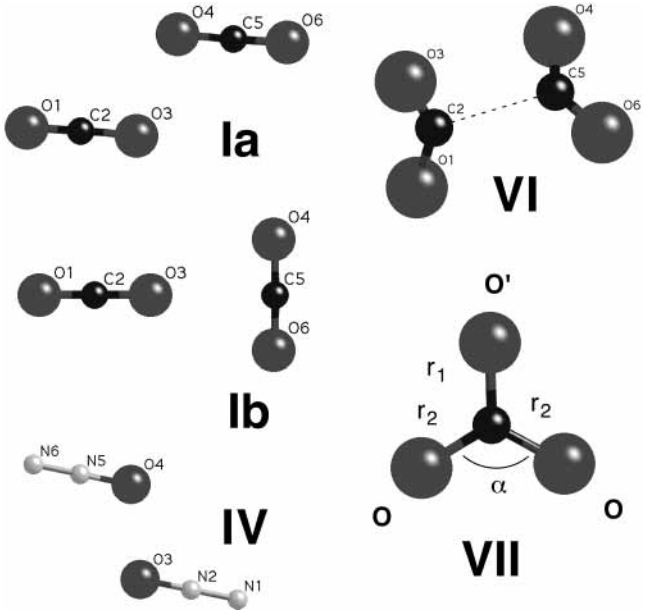


**Figure 2.** To the left: The lowest-energy geometries for the $(CO_2)_2^+$ (**Ia**, **Ib**) and $(N_2O)_2^+$ (**IV**) dimer cations in the gas phase (obtained using the B3LYP/6-31G* method). Nonplanar structures and structures with reduced symmetry have higher energies than these two conformers. See Table 1 for the geometric parameters for **Ia** and **IV** and Table 2 for the energetics of **Ib**. For **Ia**, the $X\ ^2B_u \leftarrow A\ ^2A_g$ transition dipole is in the direction of the $O_3{-}O_4$ bond. To the right: The lowest energy geometries for the $(CO_2)_2^-$ dimer anion (**VI**, $D_{2d}$, $X\ ^2A_1$) and the carbonate radical anion, $CO_3^-$ (**VII**, $C_{2v}$, $X\ ^2B_2$). In the latter anion, the symmetry is reduced from $D_{3h}$ to $C_{2v}$. For **VI**, the C−O and C−C bonds are 1.223 and 1.985 Å, respectively (vs 1.053 and 2.815 Å, respectively, in dry ice; ref 23), and the O−C−O angle is 143.6°. The Mulliken charges on the O and C atoms are −0.31 and +0.13, respectively, and the spin is 0.14 and 0.23, respectively. The hfc tensors are given in Table 1S.

(i) In contrast to the (P)MP2 and (P)MP4 calculations of McKee and co-workers (section 1S.1),[24,25] our B3LYP calculations *always* yield $C_{2h}$ symmetric "ladder" structures (**Ia**, **IIa**, and **IIIa** in Figures 2 and 3) as the *lowest* energy conformers. For this symmetry, the ground states of $(CO_2)_n^+$ cations are $^2B_u$ for even $n$ and $^2A_g$ for odd $n$. The "ladder" may be obtained by translating the monomer $CO_2$ unit in such a way that the minimum approach between the oxygens from the neighboring $CO_2$ monomers is ≈2.66 Å and the O−O−C angle is ≈100° (see Figures 2 and 3). These values may be compared to 2.3 Å and 106° in the dimer cation, structure **Ia** (Figure 2 and Table 1). The two terminal C−O bonds are stretched to 1.16 Å and the interior C−O bonds are extended to 1.18 Å (compare these two distances with the crystallographic C−O distance of 1.053 Å for $CO_2$ in dry ice).[30] Positive charge and spin are equally divided between the monomer units.

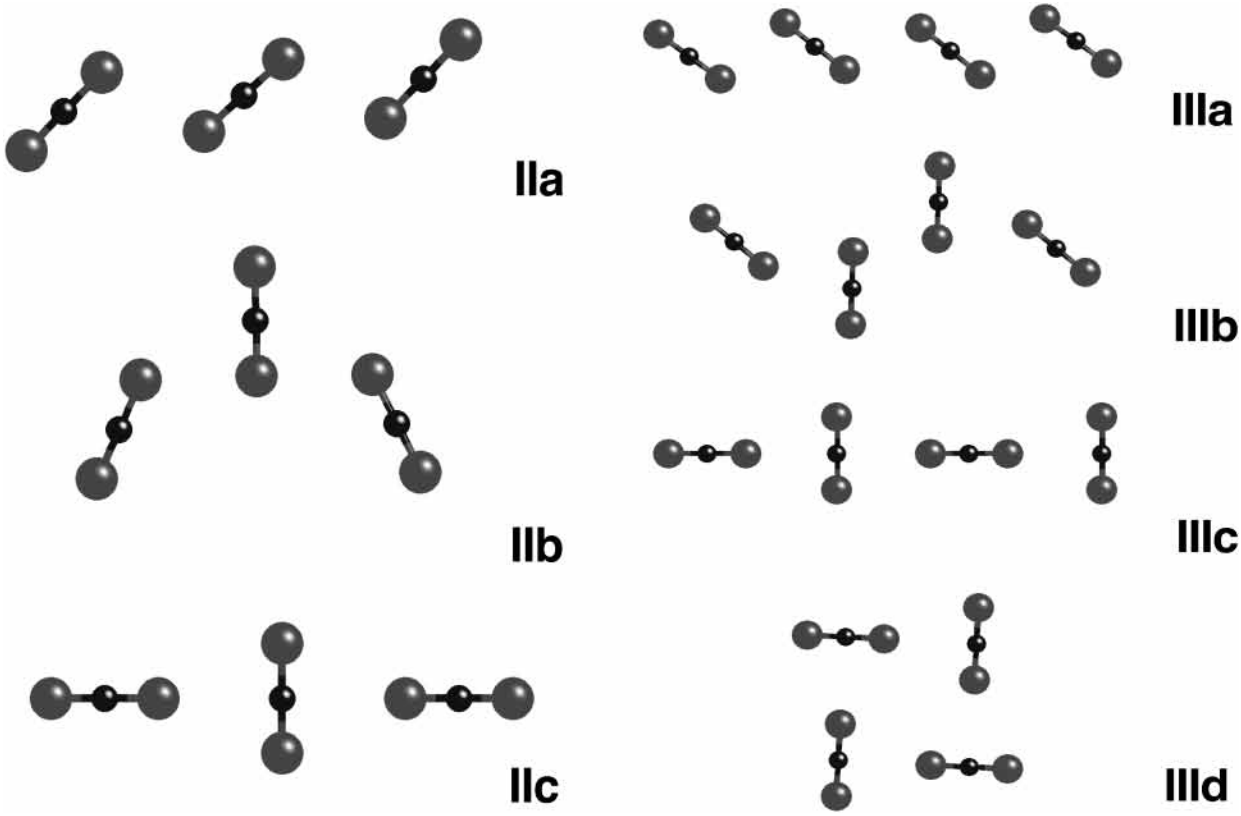


**Figure 3.** Several lowest-energy geometries for $(CO_2)_3^+$ and $(CO_2)_4^+$ cations in the gas phase (obtained using the B3LYP/6-31G* method). All of these structures are planar. See Table 2 for the energetics. To the left: For **IIa**, the minimum approach between the oxygens from different monomers is 2.56 Å and the O−O−C angle is 104.6°. In **IIc**, the minimum approach between the oxygens in the side units and the carbon atom in the central unit is 2.69 Å. In the DFT calculations, the partition of the charge/spin between the $CO_2$ units is 1:1:1 for **IIa** and 3:4:3 for **IIb** and **IIc**. In the MP2 calculations for **IIc**, the spin is on the central unit only. To the right: For **IIIa**, the minimum approach between the oxygens from different monomers is 2.66 Å and the O−O−C angles are 98° and 100°. The spin and charge are evenly divided between the monomer units. The spin densities on the oxygen atoms (starting from the terminal one) are 0.14, 0.18, 0.16, and 0.14. The C−O bond lengths vary between 1.169 and 1.177 Å.

**TABLE 1: Geometry and Charge/Spin Distributions for the Lowest Energy States of $(CO_2)_2^+$ Dimer Cations ($C_{2h}$, $X\ ^2B_u$; Structure Ia Shown in Figure 2) and Two Isoelectronic Species, $(N_2O)_2^+$ ($C_{2h}$, $X\ ^2B_u$; Structure IV Shown in Figure 2) and $(N_2O{\cdot}CO_2)^+$ ($C_s$, $X\ ^2A'$; Structure Va Shown in Figure 2S)[a]**

| cation | $(CO_2)_2^+$ | $(CO_2)_2^+$ | $(CO_2)_2^+$ | $(CO_2)_2^+$ | $(N_2O)_2^+$ | $(N_2O{\cdot}CO_2)^+$ | $(N_2O{\cdot}CO_2)^+$ |
|---|---|---|---|---|---|---|---|
| computation method | MP2 6-31G* | B3LYP 3-21G | B3LYP 6-31G* | B3LYP 6-311+G* | B3LYP 6-31G* | B3LYP 6-31G* | B3LYP 6-311+G* |
| $O_{1,6}-C_{2,5}$ | 1.155 | 1.167 | 1.157 | 1.148 | 1.131 | 1.157 | 1.148 |
| $(N_1-N_2)$[b,c] | | | | | | (1.133) | (1.125) |
| $C_{2,5}-O_{3,4}$ $(N_2-O_3)$ | 1.221 | 1.212 | 1.193 | 1.183 | 1.211 | 1.191 | 1.181 |
| | | | | | | (1.210) | (1.201) |
| $O_3-O_4$ | 2.084 | 2.156 | 2.290 | 2.320 | 2.265 | 2.283 | 2.303 |
| $\angle C_2-O_3-O_4$[b] | 99.2 | 104.2 | 106 | 107.4 | 106.9 | 112.6 | 114.4 |
| $(\angle N_2-O_3-O_4)$ | | | | | | (101.8) | (102) |
| $O_{1,6}$ $(N_1)$ (charge/spin) | −0.23/0.20 | −0.21/0.23 | −0.15/0.236 | .02/0.239 | .124/0.205 | −0.18/0.19 | −0.02/0.18 |
| | | | | | | (0.15/0.24) | (0.16/0.25) |
| $C_{2,5}$ $(N_2)$ (charge/spin) | 1.04/−0.23 | .99/−0.12 | .87/−0.104 | .53/−0.09 | .71/−0.085 | .85/−0.08 | .52/−0.07 |
| | | | | | | (0.72/−0.10) | (0.28/−0.01) |
| $O_{3,4}$ $(O_3)$ (charge/spin) | −0.31/0.53 | −0.28/0.39 | −0.22/0.368 | −0.05/0.352 | −0.33/0.38 | −0.27/0.29 | −0.12/0.27 |
| | | | | | | (−0.28/0.46) | (0.18/0.46) |
| energy, Hartree[c] | −375. | −374. | −376. | −376. | −368. | −372. | −372. |
| | 7550466 | 6196249 | 7141279 | 833017 | 903988 | 8105418 | 9237416 |
| $^2A_g$ energy, eV[d] | 2.064 | 1.405 | 0.819 | | 0.983 | | |
| osc. strength[d] | 0.265 | 0.237 | 0.151 | | 0.174 | | |

[a] All calculations are done using DFT and MP methods in Gaussian 98 (ref 29). The atoms are numbered after Figures 2 and 2S. The bond lengths are given in Å, and the angles are given in degrees; the numbers in italics are for $N_2O$ cations. The crystallographic C−O distance in the cubic dry ice is 1.053 Å. [b] The $O_1-C_2-O_2$ and $N_1-N_2-O_3$ angles are within 2° of 180°. [c] For the geometry optimized lowest energy state. [d] Vertical energy of the first excited states ($A\ ^2A_g$) relative to the ground $X\ ^2B_u$ state (in the optimum geometry) and oscillator strength for the corresponding optical transition as estimated using the CIS method from Gaussian 98.

Other side-by-side planar structures (**IIb** and **IIIb** in Figure 3) are fairly close to these "ladder" structures in energy (Table 2). Structures **IIc**, and **IIIc**, and **IIId** (Figure 3) that include T-like arranged fragments similar to **Ib** are 70−200 meV more energetic than these side-by-side structures (Table 2).

(ii) What differentiates these DFT calculations from the (P)-MP calculations of Illies et al.[24] is the partition of charge and spin between the monomers. The DFT calculations yield states in which the positive charge and spin are delocalized over the whole structure and, therefore, favor the "ladder" structures. By

**TABLE 2: Energies for the Optimum-Geometry Structures I−III of $(CO_2)_n^+$ Cluster Cations Obtained Using the B3LYP/6-31G* Density Functional Method (Gaussian 98)[29]**

| structure | symmetry[a] | ground state [b] | energy, Hartree | ΔE, meV c | −$CO_2$ dissoc. energy, eV [d] | energy per $CO_2$ molecule, Hartree |
|---|---|---|---|---|---|---|
| $CO_2$ | $D\infty h$ | $^1\Sigma_g$ | −188.5809462 | | | |
| $CO_2^+$ | $D\infty h$ | $^2\Pi_g$ | −188.0800393 | | | −188.0800393 |
| **Ia**, $(CO_2)_2^+$ | $C_{2h}$ | $^2B_u$ | −376.7141279 | 0 | 1.45 | −188.35706395 |
| **Ib** | $C_{2v}$ | $^2B_2$ | −376.7071156 | 191 | | |
| **IIa**, $(CO_2)_3^+$ | $C_{2h}$ | $^2A_g$ | −565.3147226 | 0 | 0.535 | −188.43691123 |
| **IIb** | $C_{2v}$ | $^2B_2$ | −565.3142097 | 14 | | |
| **IIc** | $D_{2h}$ | $^2B_{3g}$ | −565.3107337 | 109 | | |
| **IIIa**, $(CO_2)_4^+$ | $C_{2h}$ | $^2B_u$ | −753.9080873 | 0 | 0.338 | −188.477022[e] |
| **IIIb** | $C_{2h}$ | $^2B_u$ | −753.9068551 | 33.5 | | |
| **IIIc** | $C_{2v}$ | $^2B_2$ | −753.9052892 | 76 | | |
| **IIId** | $C_{4h}$ | $^2A_u$ | −753.9023686 | 156 | | |

[a] The symmetry specified was imposed in the calculation. [b] The lowest energy state representation. [c] The energy relative to the ladder structures **Ia**, **IIa**, and **IIIa**. [d] The heat of the cluster dissociation with the loss of a $CO_2$ molecule. [e] This energy exponentially extrapolates to −188.4873 Hartree.

contrast, the (P)MP calculations tend to localize the charge and spin either on a single monomer (as in structure **Ib**) or the pair of monomers (as in structure **Ia**). For example, although the PMP2/6-31G* calculation yields no spin on the $O_1-C_2-O_3$ fragment in **Ib** (Figure 2) and the two side monomers in **IIc** (Figure 3), the B3LYP/6-31G* calculation divides the spin as 2:3 and 3:4:3 between the corresponding monomer units. For **IIa** (Figure 3), the PMP2/6-31G* calculation places the spin on the central unit only. Because this "core" $CO_2^+$ cation repulses the $CO_2$ molecules, the PMP2 method favors the $D_{2h}$ symmetric structure **IIc** as the lowest energy state, in agreement with Illies et al. [24] For **IIIa** (Figure 3), the PMP2/6-31G* calculation places the spin on the central pair (with the O−O distance of 2.11 Å) that forms the dimer cation core; the two side monomers weakly interact with this dimer cation (the corresponding O−O distances are 2.78 Å). The repulsion between the monomer/dimer core and the $CO_2$ molecules costs energy, and T-like structures (e.g., **IIIc**) are favored as a result.

(iii) That the charge/spin sharing between the monomer units does occur for real gas-phase $(CO_2)_n^+$ cations follows from their absorption spectra. CIS calculation for the $C_{2h}$ symmetric dimer cation **Ia** yields the $A\ ^2A_g \leftarrow X\ ^2B_u$ transition in the visible that occurs when the electron in the doubly occupied subjacent $a_g$ molecular orbital no. 21 (Figure 3S(a)) is promoted from the singly occupied $b_u$ orbital no. 22 (Figure 3S(b)), as shown in Figure 3S(c). This transition can be classified as a charge resonance band in the symmetric dimer cation.[31] Because of the O−O antibonding character of the $b_u$ orbital (Figure 3S-(b)), the $A\ ^2A_g$ state is strongly repulsive. This accounts for the ease and rapidity of the $(CO_2)_2^+$ photodissociation observed in the experiments of Illies et al.[21] The corresponding transition dipole moment points in the direction of the O−O bond, in full agreement with Illies at al.[21]

Table 1 gives the estimates for the vertical energy and oscillator strength for the charge resonance transition. The MP2/6-31G* method gives the highest energy and the greatest oscillator strength (Table 1), and the B3LYP/6-31G* method gives the lowest ones. We believe that the DFT estimates are more reliable. The vertical energy of 0.82 eV and the oscillator strength of 0.151 obtained for $(CO_2)_2^+$ using the B3LYP/6-31G* method compare favorably with the experimental estimates for the onset (0.7 eV) and the oscillator strength (0.153) of the 1.63 eV band of the solvent radical cation in sc $CO_2$ (Figure 1).[1]

Similar calculations for T-like structures **Ib**, **IIc**, **IIIc**, and **IIId** (Figures 2 and 3) yield no absorbance in the visible or near-IR Although these cations have first excited states with energies ∼1 eV above their ground states (such as the $A\ ^2B_1$ state for **Ib**), the corresponding optical transitions are symmetry forbidden. The first allowed transitions involve higher excited states (such as the $C\ ^2A_1$ state for **Ib**) that have energies in excess of 5 eV. These energetics are the direct consequence of the orbital symmetry rules for these $C_{2v}$ and $D_{2h}$ symmetric structures. For the charge resonance band to form, the charge and spin must be evenly shared by the monomers. This sharing is possible only in the $C_{2h}$ symmetric "ladder" structures.

From orbital symmetry considerations, a similar charge resonance transition, $A\ ^2A_g \leftarrow X\ ^2B_u$ for even $n$ and $A\ ^2B_u \leftarrow X\ ^2A_g$ for odd $n$, should occur for all "ladder" cations. The molecular orbitals involved in this transition can be generated in the same way as those shown in Figure 3S. The electron density resides in the O 2p orbitals; the singly occupied orbital ($a_g$ for even $n$ and $b_u$ for odd $n$) has O−O antibonding character, and the subjacent orbital ($b_u$ for even $n$ and $a_g$ for odd $n$) has O−O bonding character. The charge resonance transition occurs when the electron in the subjacent orbital is promoted to the singly occupied orbital. Thus, the difference in the corresponding orbital energies is a crude estimate for the band position. For structures **Ia**, **IIa**, and **IIIa**, these differences are 2.09, 0.78, and 0.47 eV, respectively (the B3LYP/6-31G* method).

Unfortunately, the CIS method in conjunction with the B3LYP method cannot be used for higher multimers, as this method (in Gaussian 98)[29] uses the electron density obtained from a PMP2 calculation, whereas for $n > 2$, this PMP2 density is quite different from the one obtained using the DFT method, as discussed above. However, even in these MP2 calculations, the charge resonance band can be obtained for some conformations. For example, the CIS/MP2/6-31G* calculation for **IIIa** (that places the spin on the dimer at the center) yields a charge resonance band at 1.98 eV with an oscillator strength of 0.276 (compare these values with 2.06 eV and 0.265 obtained using the same method for **Ia**). Thus, a small red shift and concomitant increase in the cross-section for higher $(CO_2)_n^+$ cations observed in refs 22 and 23 could be rationalized in terms of the effect of $CO_2$ molecules on the core dimer cation, as suggested by Johnson et al.[23] On the other hand, the CIS/MP2 calculation does not yield a charge resonance band for **IIa**, which is inconsistent with the experiment of Kim et al.[22] (this band does not occur in the MP2 calculation because the spin density is placed on the middle monomer only).

Although more advanced models are needed to calculate the absorption spectra for the higher $C_{2h}$ symmetric $(CO_2)_n^+$ multimers, it is certain that these "ladder" structures exhibit a

charge resonance band that progressively red-shifts and becomes stronger as the cation size increases. Although the $C_{2h}$ symmetry might break down in large clusters (given that the energy differences between various planar side-by-side structures are less than 20−30 meV [Table 2]), the charge resonance band could persist in smaller O−O bonded fragments (as in structure **IIIb**, Figure 3). The minimum-size cation that yields this charge resonance band is the dimer cation **Ia** shown in Figure 2. The formation of a $C_{2h}$ symmetric, light-absorbing trimer cation **IIb** (Figure 3) naturally accounts for the failure of the "spectator" model for $(CO_2)_3^+$: obviously, this structure cannot be reduced to a $(CO_2)_2^+$ dimer that weakly interacts with a $CO_2$ molecule. Thus, many trends observed for the photodissociation behavior of the multimer $(CO_2)_n^+$ cations[21−23] can be accounted for by assuming that the "ladder" structures occur in such cluster cations, at least for $n \leq 6$.

With regard to the solvent cation in sc $CO_2$, it is not clear whether these extended "ladder" structures can occur in the condensed phase. We will return to this subject at the end of the next section.

**2.2. Isoelectronic Species.** $N_2O$ is a linear molecule isoelectronic with $CO_2$. Consequently, the $(N_2O)_2^+$ cation is expected to have similar geometry and electronic structure to the $(CO_2)_2^+$ dimer cation. In the gas phase, the binding energies of these two species are similar: 0.57 vs 0.67 eV, respectively.[32] $(N_2O)_2^+$ and $(N_2O{\cdot}CO_2)^+$ cations have been studied theoretically by McKee.[25] Several geometries were examined using the MP methods. McKee concluded that the lowest-energy $(N_2O)_2^+$ cation has the same $C_{2h}$ symmetry as **Ia** (structure **IV** in Figure 2).[25] Our MP2 and DFT calculations fully support this conclusion: the symmetric dimer **IV** has the lowest energy (the geometry parameters of **IV**, which are similar to those of **Ia**, are given in Table 1). One would expect that the $(N_2O{\cdot}CO_2)^+$ cation that is isoelectronic with $(N_2O)_2^+$ and $(CO_2)_2^+$ dimer cations should also have a similar structure. Instead, the calculations of McKee suggested a T-like structure **Vb** (Figure 2S) as the lowest energy state.[25]

Using the B3LYP method with the 6-31G* and 6-311+G* basis sets, we have examined several $(N_2O{\cdot}CO_2)^+$ geometries and found that the $C_s$ symmetric structure **Va** (analogous to **Ia** and **IV**) has the lowest energy (see Table 1 for the bond lengths, etc.). Other planar geometries yield cations that are >130 meV higher in energy. It appears that all three isoelectronic cations have basically the same structure. The crucial difference is that, although the $C_{2h}$ symmetric cations **Ia** and **IV** yield a charge resonance band, this does not occur for the reduced-symmetry cation **Va** (shown in Figure 2S). The ultimate cause of this changeover is the difference in the gas-phase ionization potentials for $N_2O$ and $CO_2$ (12.89 vs 13.77 eV). [33] Consequently, the spin density and the positive charge in **Va** are partitioned 0.38:0.62 in favor of the $N_2O$ fragment (Table 1). Most of this excess spin is carried by the O 2p orbital of $N_2O$ (0.46 vs 0.27 for oxygen in the $CO_2$ fragment). This disparity precludes the formation of the charge resonance band, and the bound cation absorbs such as the $N_2O^+$ monomer cation perturbed by $CO_2$.

Using the CIS/B3LYP/6-31G* method for the $(N_2O)_2^+$ dimer cation, we obtained a charge resonance band at 0.98 eV with an oscillator strength of 0.174 (vs 0.82 eV and 0.153 for $(CO_2)_2^+$; Table 1). Thus, our prediction is that the VIS band of the $(N_2O)_2^+$ cation is blue-shifted relative to that of the $(CO_2)_2^+$ cation and is slightly stronger. For the $(N_2O{\cdot}CO_2)^+$ cation, no optically allowed transition in the visible was obtained: the $B\ A' \leftarrow X\ A'$ transition (analogous to the $A\ ^2A_g \leftarrow X\ ^2B_u$ transition in the dimer cations) is at 5.5 eV. The corollary is that, although the $(CO_2)_2^+$ and $(N_2O)_2^+$ dimer cations absorb in the visible, the $(N_2O{\cdot}CO_2)^+$ cation absorbs in the UV only.

According to the mass spectrometry study of Sieck,[7] the gas-phase $(CO_2)_2^+$ cation reacts with $N_2O$ to yield a metastable $(N_2O{\cdot}CO_2)^+$ cation; the latter readily reacts with a second $N_2O$ molecule to yield the $(N_2O)_2^+$ dimer. In sc $CO_2$, the solvent radical cation reacts with $N_2O$ with a rate constant of $4.1 \times 10^{10}\ M^{-1}\ s^{-1}$ [1] which is comparable to the rate constant of charge transfer to oxygen, $3.9 \times 10^{10}\ M^{-1}\ s^{-1}$.[1,3,4] Therefore, the former reaction is likely to be a charge-transfer reaction (in the gas phase, $O_2$ has an ionization potential of 12.07 eV which is ≈0.8 eV lower than that of $N_2O$ and 1.7 eV lower than that of $CO_2$).[33] It was observed[1] that as the solvent radical cation reacts with $N_2O$, a new absorption band in the visible is formed (Figure 1S(a)). This band is observed most clearly for large concentrations of $N_2O$ (>0.1 M). However, the same band is observed at low concentrations of $N_2O$ (0.3−10 mM), and its delayed formation nearly matches the disappearance of the 1.63 eV band of the solvent radical cation. Because both the laser photoconductivity[5] and pulse radiolysis[1] experiments indicate that the solvent radical *anion* in sc $CO_2$ does not react with $N_2O$, this new band means that a *solute radical cation* is being generated. Because of the short "natural" lifetime of the solvent radical cation in sc $CO_2$ (∼50 ns),[1−4] a relatively high concentration of $N_2O$ must be added to observe the solvent cation scavenging (>0.1 mM). Given that the diffusion-controlled reactions in sc $CO_2$ exhibit rate constants of $10^{11}\ M^{-1}\ s^{-1}$,[2−5] it is impossible to conclude from the kinetic data alone whether the light-absorbing solute cation involves a single $N_2O$ molecule or two such molecules, as the $(N_2O{\cdot}CO_2)^+$ cation could rapidly dimerize with another $N_2O$ molecule, as occurs in the gas phase.

The fact that the theory yields no visible absorbance for the $(N_2O{\cdot}CO_2)^+$ cation suggests that the light-absorbing species in the $N_2O$ solutions is the $(N_2O)_2^+$ dimer. Another argument in favor of the latter species is that the band shown in Figure 1S-(a) is blue-shifted relative to that of the solvent radical cation and is 30% stronger. Both of these trends were obtained in our DFT calculation for the $(N_2O)_2^+$ dimer cation as compared to the $(CO_2)_2^+$ dimer cation (see above). Conversely, provided that the *solute* radical cation in these $N_2O$ solutions is the $(N_2O)_2^+$ dimer, the chromophore core of the *solvent* radical cation is likely to be the $(CO_2)_2^+$ dimer. Indeed, even if the formation of the multimer $(N_2O)_n^+$ cations were as rapid as that of the dimer cation, it is unlikely that these higher multimers would form in less than 10 ns, in dilute $N_2O$ solutions (1−10 mM). Thus, the close similarity between the optical spectra of the *solvent* radical cation and the *solute* $(N_2O)_2^+$ dimer cation (isoelectronic with the $(CO_2)_2^+$) suggests that the former species has a chromophore core whose electronic structure resembles that of the solute cation, namely, $(CO_2)_2^+$.

As discussed in the previous section, both the position and the oscillator strength of the charge resonance band of the $C_{2h}$ symmetric $(CO_2)_2^+$ (estimated using the CIS/B3LYP method) compare favorably with these parameters for the 1.63 eV band shown in Figure 1. We conclude that all results, experimental and theoretical, point to the $(CO_2)_2^+$ as the chromophore core of the solvent radical cation in sc $CO_2$. Although higher $C_{2h}$ symmetric multimer cations that exhibit a charge resonance band might occur in the gas phase, it seems that their formation is not favored in the liquid. Apparently, the extended "ladder" structure required for the formation of the charge resonance band is rapidly destroyed by molecular motions and collisions in the liquid.

**2.3. Solvent Radical Anion.** In Part 1 of this work,[1] the absorption spectrum of the solvent radical anion in sc $CO_2$ was obtained. This spectrum closely resembles the electron photodetachment spectrum of this species obtained in ref 5 (see also refs 34−36 and section 1S.2 in the Supporting Information). This similarity suggests that the optical absorbance is due to a bound-to-continuum electron transition to the conduction band of the solvent; there are no bound-to-bound transitions in the visible. On the other hand, it is known from the matrix isolation FTIR studies that the IR bands of $(CO_2)_2^-$ anion trapped in solid Ne and Ar matrixes can be bleached with visible light.[26] It is not clear whether this bleaching implies electron photodetachment or a photochemical reaction (e.g., C−O bond dissociation) because of a bound-to-bound transition to a repulsive state.

Because the $D_{2d}$ symmetric $(CO_2)_2^-$ dimer anion ($X\ ^2A_1$) is the most likely candidate for the core of the solvent radical anion in sc $CO_2$, we have studied this species using the CIS/6-311+G* method. In this calculation, the geometry was optimized using the B3LYP/6-311+G* method. As shown in ref 26, this geometry gives a reasonable match to the observed IR frequencies in the solid matrixes. The CIS calculation indicates that the lowest (degenerate) excited state of the anion ($A\ ^2E$) is generated when the electron in the subjacent doubly occupied *e* orbital is promoted to the singly occupied $a_1$ orbital. In the latter orbital, the unpaired electron density is in the O 2p orbitals that are oriented along the C−C bond (structure **VI**, Figure 2). Our calculation places the $A\ ^2E$ state ca. 4.5 eV above the ground state; the oscillator strength of the corresponding transition is 0.02. It seems that the dimer anion absorbs only in the UV, and this absorption is weak. No bound-to-bound transitions in the visible are possible; that is, the solvent anion band in sc $CO_2$ is indeed from a bound-to-continuum transition. Perhaps, the same type of photoexcitation occurs in the solid rare gas matrixes where the dimer anion is observed by FTIR.[26]

Interestingly, the $D_{2d}$ symmetry of the $(CO_2)_2^-$ anion is also the symmetry of pairs of neighboring $CO_2$ molecules in cubic dry ice (*Pa*3 space group, $a = 5.63$ Å).[30] The C−C distance for these pairs is 2.82 Å. As the electron is trapped, the two neighboring $CO_2$ molecules could bend and move toward each other forming a C−C bond, without symmetry-breaking rotations. On the other hand, the formation of dimer cation **Ia** in the dry ice would require such rotations.

Unfortunately, conclusive structural and mechanistic studies on the radiation-induced centers in cubic dry ice are lacking.[14] Several families of EPR signals were observed by Ikeya and co-workers.[12,13] Some of these lines were identified as resonance signals from $CO_3^-$ and $O_3^-$ radicals,[12] though only *g* tensors of these spin centers were obtained.[37] The carbonate radical anion might be formed by dissociative electron attachment, reactions 1 and 2:

$$e^- + CO_2 \rightarrow CO + O^- \quad (1)$$

$$O^- + 2\,CO_2 \rightarrow CO_3^- + CO_2 \quad (2)$$

known to occur in the gas phase.[8] The only plausible pathway to the ozonide anion, $O_3^-$,[37] would be the reaction of the $O^-$ anion generated in reaction 1 with $O_2$ impurity ($CO_3^-$ does not react with $O_2$).[38] In such a case, it is unclear (i) why the impurity center would yield the strongest signal in the EPR spectrum, (ii) how the $O_2$ impurity, given its low concentration, could efficiently compete with the $CO_2$ matrix in reaction 2, and (iii) why the yield of $O_3^-$ would *decrease* with increasing sample temperature. In the gas phase, $O_3^-$ rapidly reacts with $CO_2$ yielding $CO_3^-$ (the binding energy of $O^-$ in $CO_3^-$ is 0.58 eV higher than in $O_3^-$).[38] Given these unfavorable energetics, it is surprising that $O_3^-$ could be stable in solid $CO_2$.

Clearly, only data on hyperfine coupling (hfc) tensors can establish the identity of the radiation-induced spin centers in dry ice without ambiguity. In particular, line *C* in the EPR spectra obtained by Hirai et al.[12] (the strongest resonance signal in Figure 1, ref 12) that was rather arbitrarily[37] attributed to $O_3^-$ [12,13] closely resembles the resonance line of the $(CO_2)_2^-$ dimer anion observed in $\gamma$-irradiated $K_2C_2O_4$, where this radical anion is a hole center (only the *g* tensor of the latter center is known).[39] As discussed above, it is doubtful that the ozonide radical is the progenitor of line *C*. We believe that the $(CO_2)_2^-$ radical anion is a better candidate for such a species.

Pending more detailed EPR studies of $^{13}C$ and $^{17}O$ enriched dry ice, we looked for spectral features by which the $(CO_2)_2^-$ dimer anion can be distinguished from the $(CO_2)_2^+$ dimer cation. To this end, we calculated $^{13}C$ and $^{17}O$ hfc tensors of these two species using the B3LYP/6-311+G* method (Table 2S). It is seen that the $D_{2d}$ symmetric dimer anion exhibits large isotropic hfc constant for $^{13}C$ nuclei (twice larger than for $CO_3^-$).[18,19] This is due to strong $2\sigma p$ hybridization for the two bound C atoms; this hybridization is lacking in $CO_3^-$ and **Ia**. Another distinguishing feature is that in **VI** the long axes of $^{13}C$ and $^{17}O$ hfc tensors are parallel, whereas for **Ia** these two long axes are perpendicular. Both **Ia** and **VI** have one of the principal values of the *g* tensors close to the free electron value of 2.0023. The corresponding principal axis points in the direction of the O 2p orbitals that carry the unpaired electron.

**2.4. $CO_3^-$ Radical Anion.** The carbonate radical anion, $CO_3^-$, has been extensively studied, both theoretically[40,41] (together with isoelectronic radicals, $NO_3$ and $BO_3^{2-}$)[42−45] and experimentally.[9,10,15−20,41,44−49] (see section 1S.2 for a brief review of the data). Despite these many studies, no first-principle understanding of the light-absorbing properties, particularly in aqueous solutions, appears to exist for this radical anion.

Below we demonstrate that optical, Raman, and magnetic properties of $CO_3^-$ radicals can be consistently accounted for by the trigonally distorted, $C_{2v}$ symmetric structure **VII** (Figure 2). To this end, we performed a series of CIS/B3LYP/6-311+G* calculations in which the unique O−C−O angle α (Figure 2) was changed systematically from 110° to 140°(Figures 4−6), and the bond lengths $r_1$ and $r_2$ were optimized for every angle α (the structures obtained in the DFT calculations for related $CO_3^-$ clusters are given in Figures 7 and 8). For $\alpha = 120°$, one obtains a $D_{3h}$ geometry with the $^2A_2'$ state as the ground state. When this symmetry is relaxed to $C_{2v}$, a structure with $\alpha \approx 119.96°$ and $r_2 - r_1 \approx 10^{-4}$ Å was obtained; the energetics of the corresponding $X\ ^2B_2$ state is little different from that of the $X\ ^2A_2'$ state of the $D_{3h}$ symmetric anion. Both the CIS calculations and simple symmetry considerations indicate that these $X\ ^2B_2$ and $X\ ^2A_2'$ states do not absorb in the visible: the electron transition to the first excited state, $A\ ^2B_1$ (at 1.08 eV), is symmetry forbidden, whereas the transition to the second excited state, $B\ ^2A_1$ (with the transition dipole moment pointing in the direction of a line connecting the equivalent oxygens, Figure 2) exhibits a vertical energy of 3.6 eV and an oscillator strength $\sim 10^{-3}$. The first symmetry allowed transition is to the third excited state, $C\ ^2B_2$, with the out-of-plane transition dipole moment; this state is at 4.63 eV.

When the unique O−C−O angle α is changed from 120°, a dramatic transformation occurs (Figures 4S and 5). The energy of the optimized-geometry $CO_3^-$ anion increases as $(\alpha - 120°)^2$ (Figure 5a). The length $r_1$ of the unique C−O′ bond (Figure 2)

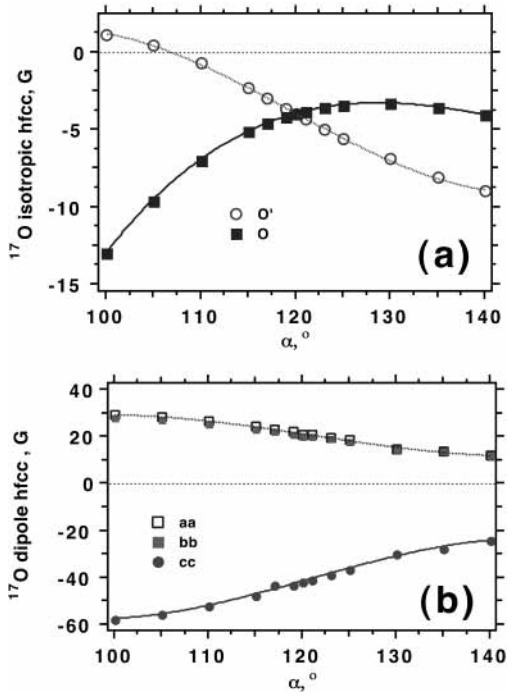


**Figure 4.** (a) Isotropic $^{17}$O hfc constants for the unique (open circles) and equivalent (filed squares) oxygens obtained using the B3LYP/6-311+G* method for the $X\ ^2B_2$ state of the $CO_3^-$ anion ($C_{2v}$ symmetry) as a function of the unique O−C−O angle α (Figure 2). The constants are given in the units of Gauss (1 G = $10^{-4}$ T). As α decreases from 120° to 110°, the hfc constant on the unique oxygen tends to zero, and the hfc constants for the two equivalent oxygens become more negative. (b) Principal values of the $^{17}$O hfc dipole tensor for the two equivalent oxygen atoms. See Table 3S for numerical values.

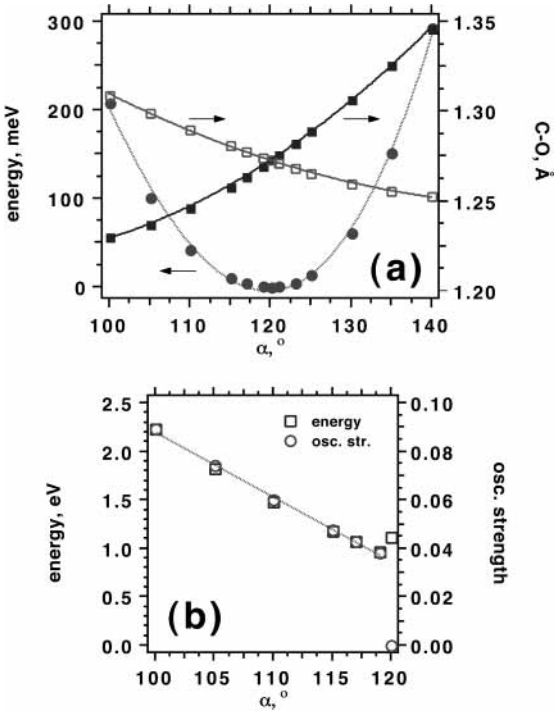


**Figure 5.** (a) Energy (filled circles) of the $X\ ^2B_2$ state of the $CO_3^-$ anion ($C_{2v}$ symmetry) as a function of O−C−O angle α between the equivalent oxygens (Figure 2). The energy obtained using the B3LYP/6-311+G* method is given with respect to the $X\ A_2'$ state of the $D_{3h}$ symmetric anion. The C−O′ distance $r_1$ (filled squares) and C−O distance $r_2$ (empty squares) introduced in Figure 2 are shown in the same plot. See Table 3S for numerical values. (b) Vertical energy (empty squares) and oscillator strength (empty circles) for the $X\ ^2B_2 \leftarrow A\ ^2A_1$ optical transition as a function of angle α. These parameters were estimated using the CIS/6-311+G* method for the B3LYP/6-311+G* optimized geometries.

increases with α (Figure 5a), and the length $r_2$ of the two C−O bonds decreases with α. For smaller angles α, the charge on the unique oxygen atom becomes more negative (Figure 4S), and the C−O′ bond becomes more like C−O$^-$. The spin density on the two equivalent O atoms increases and that on the O′ atom decreases for more acute angles α (Figure 4S). These trends are understandable: as the O−C−O angle decreases, the repulsion between the two equivalent oxygens becomes stronger. To minimize this repulsion, the charge on these oxygens becomes *less* negative and the charge on the unique oxygen *more* negative. As the electron density on the O′ atom increases, the unpaired electron density shifts toward the O 2p orbitals.

As shown in Figure 5b, there is a strong correlation between the trigonal distortion and the position and the strength of the absorption band in the visible. The $X\ ^2B_2$ state remains the ground state for all angles α, but the energetics of the excited states changes. For angles α lower than 119°, the $^2A_1$ (0.9−2.2 eV) and $^2B_1$ states (>2.7 eV) are the first and the third excited states (that dissociate to $CO_2 + O^-$). This is in full agreement with the energy diagram sketched for the $CO_3^-$ moiety in $CO_3^-(H_2O)_{1-3}$ anions by Castleman et al.[46] The $^2A_2$ state is predicted to be the second excited state (that dissociates to $CO_2^- + O$).[46] Optical transitions to these $B\ ^2A_2$ and $C\ ^2B_1$ states are forbidden by symmetry. The $A\ ^2A_1$ state is obtained by promoting the electron in the doubly occupied subjacent $a_1$ molecular orbital no. 15 to the singly occupied $b_2$ orbital no. 16. The resulting optical transition is allowed by symmetry, and the transition dipole moment is oriented between the two equivalent oxygens, in agreement with ref 41. This dipole moment decreases with α because less electron density resides in the O′ 2p orbital of the corresponding $A\ ^2A_1$ state. Consequently, both the oscillator strength ($f$) and the vertical energy of the $A\ ^2A_1 \leftarrow X\ ^2B_2$ transition increase as α decreases (Figure 5b). For α = 119°, $f \approx 0.038$ and the band energy is 0.97 eV, whereas for α = 100°, $f \approx 0.09$ and the band energy is 2.27 eV. Experimentally,[9,10] the VIS band of aqueous $CO_3^-$ exhibits an onset at 1.5 eV and $f \approx 0.042$ (Figure 1S(b)). Using Figure 5b, one finds that this onset corresponds to α ≈ 110° for which $f \approx 0.06$. Thus, both the band position and the oscillator strength can be accounted for by a trigonally distorted anion **VII**. Does such a distortion account for other properties of $CO_3^-$?

First, consider the EPR parameters.[16−19,41] The hfc tensors for $^{13}$C and $^{17}$O nuclei of the carbonate radical as a function of α are given in Table 3S and Figure 4. The EPR data for $CO_3^-$ in $KHCO_3$[17] (in which the symmetry is reduced to $C_s$ by the crystal field) indicate that the spin density on one of the oxygens is virtually zero, whereas two other oxygens-17 exhibit isotropic hfc constants of −9.95 and −16.2 G (1 G = $10^{-4}$ T). The principal values for the corresponding (nearly axial) dipole hfc tensors are (+17, +21.5, −38.5) G and (+38.7, +30.6, −69.2) G.[17] Taking the median of these two hfc tensors (for a hypothetical $C_{2v}$ symmetrical structure), we obtain the isotropic constant of −13.2 G and the **cc** value of the dipole tensor of −53.9 G. The hfcc coupling tensors for $^{13}$C were determined in several host crystals (see Table 1 in ref 18 and the compilation of the EPR data in ref 19). With the exception of $CO_3^-$ in KCl,[18] the isotropic hfc constants are ca. −11.5 G, and the typical values for the dipole tensor are (+1.3, +1.3, −2.6) G.[18,41] The $g$-tensor analyses carried out in ref 18 suggested that in most host crystals the carbonate radical has the $C_{2v}$ symmetry and α ≈ 90−110°. An estimate of α ≈ 100° was obtained in the INDO calculations of ref 40, though no hfc parameters were given.

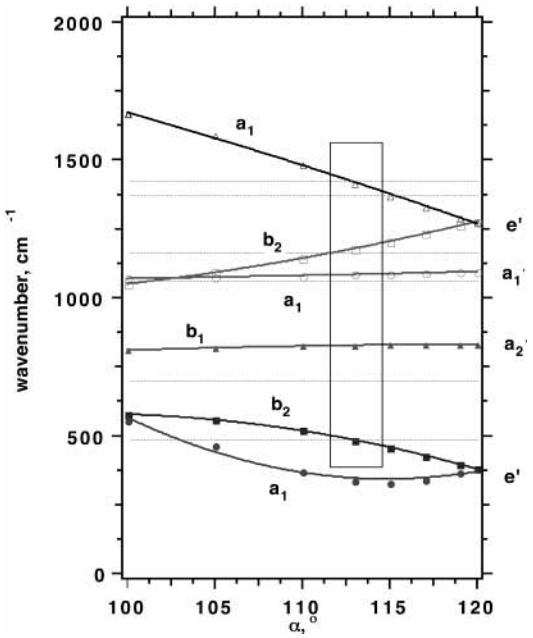


**Figure 6.** Normal modes (see Table 3) for the ground-state $CO_3^-$ anion ($C_{2v}$ symmetric structure **VII**) as a function of the unique O−C−O angle α. As this angle tends to 120°, the $a_1$ and $b_2$ modes collapse to the doubly degenerate $e'$ mode. The horizontal straight lines are experimental Raman data from ref 15. The best match (highlighted by the rectangle) is for α ≈ 113°. Note that the out-of-plane $b_1$ mode is Raman-forbidden. The 701 $cm^{-1}$ mode could be a combined lowest-frequency $a_1$ mode. Note that the frequency of the symmetric $a_1$ (breathing) mode $\nu_4$ weakly depends on the O−C−O angle.

The angular dependencies for the $^{17}O$ isotropic hfc constants for the unique (O′) and two equivalent oxygens (O) are shown in Figure 4a. The $^{17}O'$ constant approaches zero for α ≈ 100−105°, whereas the $^{17}O$ constant becomes more negative as α decreases. This behavior is consistent with the trends shown in Figure 4S. Figure 4b demonstrates the angular dependence for the principal values of the dipole hfc tensor of the equivalent $^{17}O$ nuclei. The best match to the observed $^{17}O$ hfc tensor is obtained for α = 100°: the isotropic hfc constant of −13 G and the dipole hfc tensor of (+29.5, +28.2, −57.6) G. For this α, the isotropic hfc constant on $^{13}C$ is −11.6 G, and the dipole hfc tensor is (+1.46, +1.54, −3) G. Both of these $^{13}C$ and $^{17}O$ hfc tensors compare favorably with the experimental ones.[17,18,41] As discussed above, our estimate is also consistent with the estimates of α obtained from the *g*-tensor analyses.[18] It seems that in crystalline matrixes the $CO_3^-$ radical is strongly distorted. In aqueous solution, less distortion is expected.

The Raman spectrum of aqueous $CO_3^-$ was obtained by Bisby et al. (Table 3).[15] The most prominent band (1063 $cm^{-1}$) corresponds to the symmetric C−O stretch (the breathing mode of the carbonate radical anion). In addition, four weaker and broader bands were observed at 485, 701, 1166, and ∼1400 $cm^{-1}$.[15] The latter band was decomposed into the 1372 and 1426 $cm^{-1}$ subbands. Bisby et al. argue,[15] in analogy to the Raman spectrum of aqueous $CO_3^{2-}$, that the band splitting is caused by solvent−solute interaction. From general considerations,[15] these five Raman bands were classified as shown in Table 3, column 3. Provided that this classification is correct, it is difficult to rationalize why the symmetry-forbidden $b_1$ band (that corresponds to antisymmetric out-of-plane mode) would be more prominent than the symmetry-allowed $a_1$ and $b_2$ bands.

The angular dependence for the normal-mode frequencies of **VII** is shown in Figure 6. As the angle α decreases from 120°, the two degenerate $e'$ modes split into the $a_1$ and $b_2$ modes.

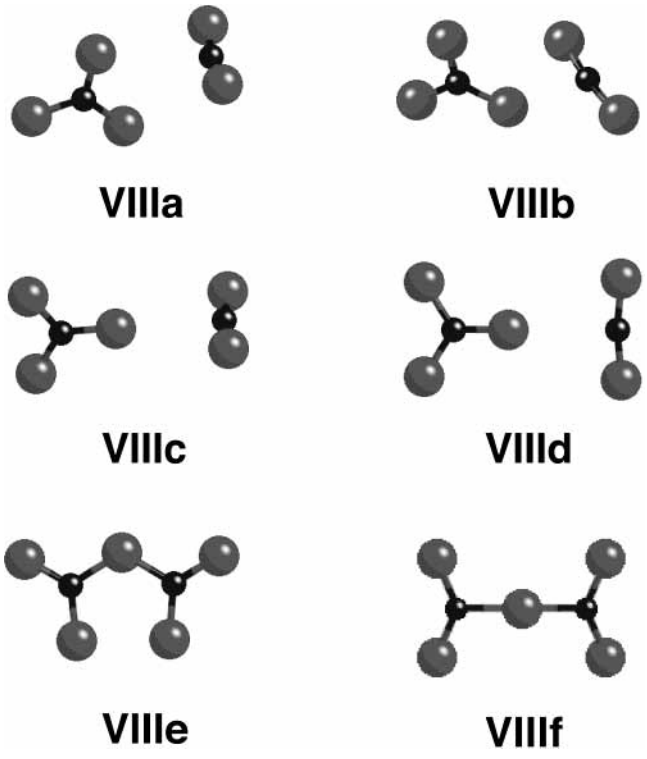


**Figure 7.** Several possible structures for the $CO_3^-{\cdot}CO_2$ anion (geometry-optimized using the B3LYP/6-31G* method; see also Table 2S). Covalently bound $C_2O_5^-$ anions **VIIIe** and **VIIIf** are not favored energetically. In structures **VIIIa**−**VIIId**, the negative charge and spin reside on the $CO_3^-$ moiety. $C_s$ symmetric nonplanar structures **VIIIa** and **VIIIb** exhibit lower energies than $C_{2v}$ symmetric structures **VIIIc** and **VIIId**. For **VIIIa** and **VIIIf**, there are no optical transitions in the visible. For structures **VIIIb**−**VIIId**, the unique O−C−O angle is reduced to 116−118°, and there are optical transitions at 0.95−1.05 eV with the oscillator strengths of (3−3.5) × $10^{-2}$. For **VIIIe**, there is a strong optical transition to the first excited $^1A_2$ state at 2.28 eV with an oscillator strength of 0.16.

The frequencies of the breathing $a_1$ mode and the out-of-plane $b_1$ mode depend weakly on the O−C−O angle. Although the frequencies of the $a_1$ mode compare well with the 1063 $cm^{-1}$ band observed experimentally, the 700 $cm^{-1}$ Raman band cannot be related to the (symmetry-forbidden) $b_1$ mode, as the latter should have higher frequency and low intensity. Actually, as shown in Figure 6, *all five* Raman-active bands observed by Bisby et al.[15] can be matched with the modes given by our DFT calculation provided that (i) the modes are classified as shown in Table 3, column 1, (ii) an O−C−O angle of 112−113° is assumed, and (iii) the 700 $cm^{-1}$ band is regarded as a combined ($2\nu_1$) mode resulting from the symmetry-allowed $a_1$ vibration. The frequencies for the α = 113° anion are given in Table 3, column 4. For this O−C−O angle, the $A\ ^2A_1 \leftarrow X\ ^2B_2$ transition is predicted to have a vertical energy of 1.3 eV and an oscillator strength of 0.05. Both of these estimates are reasonably close to 1.4−1.5 eV and 0.042, respectively, observed for aqueous $CO_3^-$.[9,10]

Thus, both the optical and Raman properties of aqueous $CO_3^-$ can be consistently accounted for assuming a $C_{2v}$ symmetric structure **VII** with α ≈ 113°, whereas the EPR data for $CO_3^-$ centers in carbonate crystals suggest more distorted species with α ≈ 100°. No complexation between the $CO_3^-$ and $CO_3^{2-}$ postulated in ref 11 is needed to explain these properties. Perhaps, the changes observed in the UV−vis spectra of $CO_3^-$ in hot and supercritical water[11] actually result from slight changes in the equilibrium O−C−O angle rather than com-

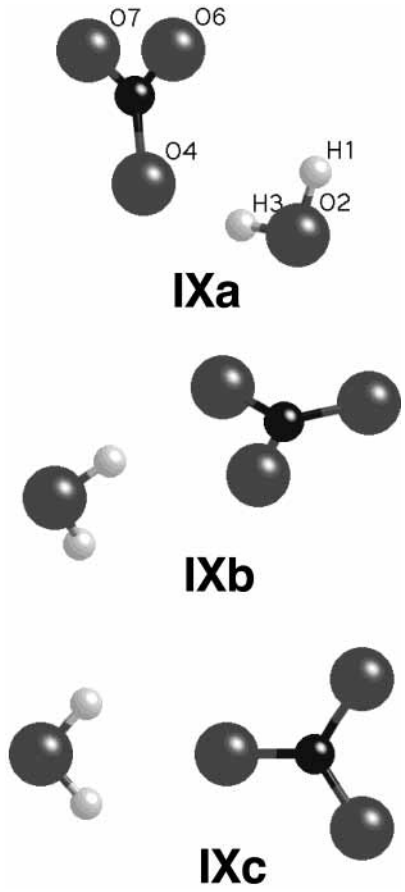


**Figure 8.** Several possible structures for the $CO_3^-\cdot H_2O$ anion (geometry-optimized using the B3LYP/6-31G* method; see Table 2S and 3S). In the lowest-energy $C_s$ symmetric structure **IXa**, the water molecule forms a single anion H-bond with the $CO_3^-$ moiety (the O−H distance is 1.8 Å); in **IXb** and **IXc**, there are two weak hydrogen bonds (the O−H distances are 2.24 Å and 2.16 Å, respectively).

plexation with (bi-)carbonate anion (though a hydrogen-bonded compex of $CO_3^-$ with $HOCO_2^-$ is, in principle, possible).

Our examination would be incomplete without answering the question as to how the polar medium, e.g., liquid water, causes symmetry breaking in $CO_3^-$. As seen from Figure 5a, in the gas phase, there is a considerable penalty for the trigonal distortion. For instance, the $C_{2v}$ symmetric anion with $\alpha = 110°$ is 50 meV more energetic than the $D_{3h}$ symmetric anion with $\alpha = 120°$. We argue that, in water, the trigonal distortion is favored because it increases the negative charge on the unique oxygen atom; as a result, ionic hydrogen bonding[50] involving this oxygen becomes stronger. This point is demonstrated by DFT calculations (B3LYP/6-31G* method) for $CO_3^-\cdot H_2O$ clusters shown in Figure 8. Several possible geometries for these clusters were examined. The $C_s$ and $C_{2v}$ symmetric anions shown in Figure 8 have the lowest energies (Table 2S). In all three of these anions, (i) the negative charge and spin reside on the $CO_3^-$ moiety, (ii) the water molecule is hydrogen-bonded to a single oxygen atom, and (iii) the angle between two "loose" oxygen atoms is reduced (see Figure 8 and Table 3S), so that the $CO_3^-$ anion exhibits $C_{2v}$ symmetry. The strongest hydrogen bond with an O−H distance of 1.8 Å was obtained for the lowest-energy $C_s$ symmetric structure **IXa**, for which $\alpha \approx 117.5°$. Table 3 lists the frequencies of the normal modes (C−O vibrations only) for this anion. These frequencies are fairly similar to the ones obtained for **VII** with the same unique O−C−O angle α. In the $C_{2v}$ symmetric structure **IXc** (which is 70 meV more energetic than **IXa**), there are *two* hydrogen bonds (the O−H distance is 2.16 Å). These bonds are weaker than in **IXa**, but the charge on the H-bound oxygen is more negative than in **IXa** (−0.58 vs −0.55), and consequently, the O−C−O angle is reduced to 114.4°. This angle is close to $\alpha \approx 113°$ favored by the mode matching analysis in Figure 6, and predictably, similar frequencies of the normal modes are obtained (Table 3). The formation of the hydrogen bond in **IXa** agrees with the substantial binding energy (−0.61 eV) obtained for the $CO_3^-\cdot H_2O$ anion in the gas phase.[47] We stress that the energy difference between the conformers $CO_3^-\cdot H_2O$ shown in Figure 8 is small (<70 meV), and these conformers may coexist in liquid water.

Of course, many different bonding arrangements for the hydrated $CO_3^-$ anion may exist in aqueous solution. However, it is likely that this species can only bind strongly to a *single* water molecule. Indeed, as soon as the hydrogen bond is formed, the charge density on the two spin-bearing oxygens decreases markedly (Figure 4S), and subsequent hydrogen bonding becomes less efficient. Experimentally, addition of extra water molecule(s) decreases the bond dissociation energy of the $CO_3^-(H_2O)_n$ anion from −0.61 to −0.57 eV,[51] and only $CO_3^- + nH_2O$ photodissociation is observed for $n = 2$ and $n = 3$ anions.[46] This total loss of water ligands suggests that additional water molecules form hydrogen bonds with each other rather than the $CO_3^-$ anion.[51] Thus, we envision the aqueous $CO_3^-$ as a core $CO_3^-\cdot H_2O$ anion that *relatively weakly* interacts with other water molecules; this explains the similarity between the photodestruction spectra of $CO_3^-\cdot H_2O$[45] and the optical spectra of aqueous $CO_3^-$.[9,10] The degree of trigonal distortion observed for the $CO_3^-$ moiety in the gas-phase $CO_3^-\cdot H_2O$ anion is sufficient to account for the VIS and Raman properties of aqueous $CO_3^-$. It seems reasonable that this core anion is also present in the supercritical water.[11]

We turn now to $CO_3^-$ in supercritical $CO_2$. Dissociative electron capture (concerted reactions 1 and 2) is known to occur for $(CO_2)_2$ clusters in the gas phase[8] and, possibly, in dry ice.[12−14] The involvement of $O^-$ or $CO_3^-$ had also been postulated to account for radiation-induced oxidation of aromatic hydrocarbons in liquid $CO_2$ at −18 °C.[52] On the other hand, in radiolysed sc $CO_2$, no $CO_3^-$ anions were observed by UV−vis spectroscopy.[1−5] Charge balance considerations discussed in ref 1 suggest that, in sc $CO_2$, the fraction of ionization events yielding the $CO_3^-$ anion is <3%. As an upper limit, 10−20% of the anions present after a 10 ns fwhm electron beam pulse would be $CO_3^-$ anions. Could it be that this species escaped observation because the carbonate radical anion in sc $CO_2$ is a poor light absorber? Here, we consider the following two possibilities: (i) that $CO_3^-$ does not exist in sc $CO_2$ and (ii) that the trigonal distortion of $CO_3^-$ in sc $CO_2$ is weak and the $^2A_1 \rightarrow X\ ^2B_2$ band is lacking. The first possibility seems unlikely as the experimental data for $CO_3^-(CO_2)_n$ cluster anions[48] give low binding energies for these anions that range from 0.26 eV for $n = 1$ to 0.19 eV for $n = 8$.

Using the B3LYP/6-31G* method, we examined several structures for the $(CO_3\cdot CO_2)^-$ complex. The formation of covalently bound planar $C_2O_5^-$ structures **VIIIe** and **VIIIf** (Figure 7) is not favored energetically (Table 2S). The $C_{2v}$ symmetric structure **VIIIe** ($X\ ^2B_2$) is 170 meV more energetic than the lowest-energy structure **VIIIa**; it also strongly absorbs in the visible, with the $A\ ^2A_1 \leftarrow X\ ^2B_2$ band at 2.28 eV and $f \approx 0.16$. If **VIIIe** were to form in radiolysed sc $CO_2$, it would have been observed. Apparently, no covalently bound $C_2O_5^-$ anions are formed due to the unfavorable energetics.

In structures **VIIIa**−**VIIId**, the negative charge resides on the $CO_3^-$ moiety, and the latter weakly interacts with a

**TABLE 3: Vibration Frequencies ($cm^{-1}$) for the $CO_3^-$ Moieties in $CO_3^-$ ($C_{2v}$) and $H_2O{\cdot}CO_3^-$ Anions (structures IXa and IXc in Figure 8) Calculated Using the B3LYP/6-311+G and B3LYP/6-31G* Methods, Respectively, Compared with the Time-Resolved Raman Spectroscopy Data of Ref 15**

| normal mode | expt[15] | *a* | $CO_3^-$ **VII**, $\alpha = 113°$[b] | $H_2O{\cdot}CO_3^-$ **IXa**, $\alpha = 117.5°$ | $H_2O{\cdot}CO_3^-$ **IXc**, $\alpha = 114.4°$ | type |
|---|---|---|---|---|---|---|
| $\nu_1(a_1)$ | 350 (?)[c] | $a_1$ | 335 | 326 | 347 | C−O symm. |
| $\nu_2(b_2)$ | 485 | $b_1$ | 483 | 418 | 487 | C−O antisymm. |
| $\nu_3(b_1)$ | 701 (?)[d] | $a_1$ | 828 | 828 | 815 | out of plane |
| $\nu_4(a_1)$ | 1063[e] | $a_1$ | 1085 | 1107 | 1106 | C−O breathing |
| $\nu_5(b_2)$ | 1166 | $a_1$ | 1178 | 1271 | 1225 | C−O antisymm. stretch |
| $\nu_6(a_1)$ | 1372, 1426[f] | $b_2$ | 1413 | 1371 | 1484 | C−O symm. stretch[g] |

[a] Mode symmetries suggested in ref 15. [b] Optimum O−C−O angle estimated from the mode-matching plot in Figure 6. [c] Assuming that the 701 $cm^{-1}$ mode is a combined $\nu_1$(a) mode. [d] Assuming that the 701 $cm^{-1}$ mode is a Raman-forbidden out-of-plane mode. [e] A symmetric C−O stretching $a_1$ mode as suggested by the polarization. [f] In ref 15, the splitting of the band in two subbands is explained by interaction with the solvent, in a fashion similar to the previously studied $CO_3^{2-}$ anion. [g] This mode primarily involves the C−O stretch for the unique oxygen.

"spectator" $CO_2$ molecule. In all of these structures, the $CO_3^-$ anion is trigonally distorted because of the repulsion between the $CO_3^-$ anion and the $CO_2$ molecule, although this distortion is weak. (Hiraoka and Yamaba[48] regard the $n = 1-3$ cluster anions as bound by weak "chelate bonds" between the $CO_2$ carbons and $CO_3^-$ oxygens with bond lengths of $\approx 2.7$ Å, but whether the observed trigonal distortion results from the formation of these bonds or because of the repulsion between the $CO_2$ and $CO_3^-$ oxygens is not settled.) In structures **VIIIb**−**VIIIc**, the unique O−C−O angle $\alpha \approx 117-119°$, and the corresponding anions absorb in the visible (with a band onset at 0.9−1 eV and an oscillator strength ~0.03). In the lowest-energy $C_s$ symmetric structure **VIIIa**, the repulsion between this anion and the $CO_2$ molecule leads to $\alpha > 120°$ (namely, $\alpha \approx 125.5°$) and this structure does not absorb in the visible. Hiraoka and Yamabe [48] obtained the same structure **VIIIa** in their MP2/6-31+G*//RHF/6-31+G* calculation. According to their study, the $n = 2$ and 3 anions also have the $C_{2v}$ symmetry with $CO_2$ molecules perpendicular to the $CO_3^-$ plane (see Figure 6 in ref 48); in these structures, $\alpha \approx 105.6°$ (vs $\alpha \approx 113.3°$ that they obtained for $CO_3^-$).

We conclude that in, sc $CO_2$, the carbonate radical anion should have the same $CO_3^-$ core as in polar matrixes. Because the trigonal distortion in this radical anion is mainly due to weak O−O repulsion (or C−O "chelate bonding")[48] between the $CO_3^-$ core and $CO_2$ molecules, we expect this distortion to be small. For the $CO_3^-{\cdot}CO_2$ anion, the lowest-energy conformation yields the least O−O repulsion and no visible absorbance. Snodgrass et al.[47] found that the $CO_3^-{\cdot}CO_2$ and $CO_3^-{\cdot}H_2O$ anions have similar photodestruction spectra in the 2.1−2.7 eV region, but the former anion has 1.5−2 times lower cross section. Thus, for $CO_3^-$ in sc $CO_2$ we expect to find a weak, possibly red-shifted absorption band. It is conceivable that this band is swamped by much stronger absorption of the solvent radical cation (at early delay times) and, at later delay times, by the absorbance of a neutral product (as discussed in ref 1).

## 3. Conclusions

Several radical cations and anions have been examined theoretically using density functional calculations for comparison with structural studies on the solvent radical ions generated in pulse radiolysis of supercritical $CO_2$. The following conclusions have been reached:

(1) In the gas phase, the lowest energy $(CO_2)_n^+$ cations exhibit the $C_{2h}$ symmetric "ladder" structure; the spin and charge are uniformly spread between the monomer units. The charge resonance band of these multimer cations involves their $^2B_u$ and $^2A_g$ states. In the first excited state, the doubly occupied HOMO has O−O antibonding character which accounts for the ease of photodissociation.[21] The absorption band shifts to the red with the cation size. For the $(CO_2)_2^+$ cation, the position and the oscillator strength of this charge resonance band are similar to those determined for the solvent radical cation in radiolyzed sc $CO_2$.[1] The formation of these "ladder" structures can account for several trends observed experimentally in the photodestruction spectra of $(CO_2)_n^+$ clusters.[21−23]

(2) The radical cation species observed in pulse radiolysis of $N_2O$ solutions in sc $CO_2$ is the $(N_2O)_2^+$ dimer cation which is isoelectronic with the $(CO_2)_2^+$ dimer cation. These two cations have similar structures and energetics. For the $(N_2O{\cdot}CO_2)^+$ cation, no charge resonance band is obtained, because of the localization of positive charge on the $N_2O$ moiety. The striking similarity between the spectrum of the $(N_2O)_2^+$ dimer cation and the solvent cation in sc $CO_2$[1] suggests that the $(CO_2)_2^+$ dimer is the chromophore core of the solvent radical cation in this liquid. Apparently, extended "ladder" multimers do not occur (or do not prevail) in solution.

(3) It is shown that the $D_{2d}$ symmetric $(CO_2)_2^-$ dimer anion (expected to be the core of the high-mobility solvent radical anion in sc $CO_2$)[5] exhibits no bound-to-bound transitions in the visible. The experimentally observed band with onset at 1.76 eV is due to a bound-to-continuum transition of the electron to the conduction band of the solvent. This conclusion agrees well with the dc conductivity studies of ref 5. It is predicted that the $(CO_2)_2^-$ dimer anion will occur as a stable electron center in dry ice; the calculated EPR parameters for the $(CO_2)_2^-$ and $(CO_2)_2^+$ are given in Table 1S. Perhaps, the dimer anion in dry ice has already been observed in the EPR studies of Ikey and co-workers.[12,13,14]

(4) It is shown that optical,[9,10] Raman,[15] and EPR spectra[16−19] of the carbonate radical anion, $CO_3^-$, are consistent with the $C_{2v}$ symmetric structure **VII** with an O−C−O angle of ≈113° (in the aqueous solution). This angle is reduced to 100° for the hole centers ($CO_3^-$ radicals) occurring in $\gamma$-irradiated carbonate minerals. Our calculations indicate that the oscillator strength of the optical transition in the visible strongly correlates with the trigonal distortion: as the O−C−O angle gets more acute, the absorption becomes more efficient and it occurs at higher photon energies. In aqueous solution, the trigonal distortion is due to ionic hydrogen bonding[50] of the carbonate radical anion to a single water molecule. In sc $CO_2$ (and other nonpolar liquids), trigonal distortion might also occur, because of repulsion between the $CO_3^-$ anion and the solvent molecules. However, this repulsion is weak, and we predict that in these nonpolar media the carbonate radical anion is a poor light absorber in the visible.

**Acknowledgment.** I.A.S. thanks Drs. C. D. Jonah, D. M. Bartels, T. Marin, M. C. Sauer, Jr., R. A. Crowell, and S.

Pommeret for stimulating discussions and technical assistance. This work was performed under the auspices of the Office of Basic Energy Sciences, Division of Chemical Science, US-DOE under Contract No. W-31-109-ENG-38.

**Supporting Information Available:** 1. Background; 2. Captions to Figures 1S−4S; 3. Tables 1S−3S. 3. Figures 1S−4S. This material is available free of charge via the Internet at http://pubs.acs.org.

## References and Notes

(1) Shkrob, I. A.; Sauer, M. C., Jr.; Jonah, C. D.; Takahashi, K. *J. Phys. Chem. A* **2002**, *106*, 11855.

(2) Dimitrijevic, N. M.; Bartels, D. M.; Jonah, C. D.; Takahashi, K. *Chem. Phys. Lett.* **1999**, *309*, 61.

(3) Dimitrijevic, N. M.; Takahashi, K.; Bartels, D. M.; Jonah, C. D.; Trifunac, A. D. *J. Phys. Chem. A* **2000**, *104*, 568.

(4) Takahashi, K.; Sawamura, S.; Dimitrijevic, N. M.; Bartels, D. M.; Jonah, C. D. *J. Phys. Chem. A* **2002**, *106*, 108.

(5) Shkrob, I. A.; Sauer, M. C., Jr. *J. Phys. Chem. B* **2001**, *105*, 4520.

(6) Smith, G. P.; Lee, L. C. *J. Chem. Phys.* **1978**, *69*, 5393

(7) Sieck, L. W. *Int. J. Chem. Kinet.* **1978**, *10*, 335.

(8) Klots, C. E.; Compton, R. N. *J. Chem. Phys.* **1978**, *69*, 1636.

(9) Weeks, J. L.; Rabani, J. *J. Phys. Chem.* **1966**, *70*, 2100.

(10) Behar, D.; Czapski, G.; Duchovny, I. *J. Phys. Chem.* **1970**, *74*, 2206.

(11) Wu, G.; Katsumura, Y.; Muroya, Y.; Lin, M.; Morioka, T. *J. Phys. Chem. A* **2002**, *106*, 2430.

(12) Hirai, M.; Ikeya, M.; Tsukamoto, Y.; Yamanaka, C. *Jpn. J. Appl. Phys.* **1994**, *55*, L1453

(13) Tsukamoto, Y.; Ikeya, M.; Yamanka, C. *Appl. Radiat. Isot.* **1993**, *44*, 221; **2000**, *52*, 1259.

(14) Wu, G. *Appl. Radiat. Isot.* **2001**, *55*, 895. Norizawa, K.; Kanosue, K.; Ikeya, M. *Appl. Radiat. Isot.* **2001**, *55*, 896.

(15) Brisby, R. H.; Johnson, S. A.; Parker, A. W.; Tavender, S. M. *J. Chem. Soc., Faraday Trans.* **1998**, *94*, 2069. Tavender, S. M.; Johnson, S. A.; Balsom, D.; Parker, A. W.; Bisby, R. H. *Laser Chem.* **1999**, *19*, 311.

(16) Atkins, P. W.; Symons, M. C. R. *The structure of Inorganic Radicals*; Elsevier: New York, 1967; p 162.

(17) Top, Z. H.; Raziel, S.; Luz, Z.; Silver, B. L. *J. Magn. Reson.* **1973**, *12*, 102.

(18) Moens, P.; Callens, F.; Boesman, E. *J. Phys. Chem. Solids* **1995**, *56*, 813.

(19) Hisatsune, I. C.; Adl, T.; Beahm, E. C.; Kempf, R. J. *J. Phys. Chem.* **1970**, *74*, 3225.

(20) Chawla, O. P.; Fessenden, R. W. *J. Phys. Chem.* **1975**, *79*, 2693.

(21) Illies, A. J.; Jarrold, M. F.; Wagner-Redeker, W.; Bowers, M. T. *J. Phys. Chem.* **1984**, *88*, 5204.

(22) Kim, H.-S.; Jarrold, M. F.; Bowers, M. T. *J. Chem. Phys.* **1986**, *84*, 4882.

(23) Johnson, M. A.; Alexander, M. L.; Lineberger, W. C. *Chem. Phys. Lett.* **1984**, *112*, 285.

(24) Illies, A. J.; McKee, M. L.; Schlegel, H. B. *J. Phys. Chem.* **1987**, *91*, 3489.

(25) McKee, M. L. *Chem. Phys. Lett.* **1990**, *165*, 265

(26) (a) Zhou, M.; Andrews, L. *J. Chem. Phys.* **1999**, *110*, 6820. (b) Zhou, M.; Andrews, L. *J. Chem. Phys.* **1999**, *110*, 2414. Thompson, W. E.; Jacox, M. E. *J. Chem. Phys.* **1999**, *111*, 4487; *J. Chem. Phys.* **1989**, *91*, 1410.

(27) Møller, C.; Plesset, M. C. *Phys. Rev.* **1934**, *46*, 618. Frish, M. J.; Head-Gordon, M.; Pople, J. A. *Chem. Phys. Lett.* **1988**, *153*, 503; **1990**, *166*, 275; **1990**, *166*, 281.

(28) Becke, A. D. *Phys. Rev. A* **1988**, *38*, 3098. Lee, C.; Yang, W.; Parr, R. G. *Phys. Rev. B* **1988**, *37*, 785

(29) Frisch, M. J.; Trucks, G. W.; Schlegel, H. B.; Scuseria, G. E.; Robb, M. A.; Cheeseman, J. R.; Zakrzewski, V. G.; Montgomery, J. A., Jr.; Stratmann, R. E.; Burant, J. C.; Dapprich, S.; Millam, J. M.; Daniels, A. D.; Kudin, K. N.; Strain, M. C.; Farkas, O.; Tomasi, J.; Barone, V.; Cossi, M.; Cammi, R.; Mennucci, B.; Pomelli, C.; Adamo, C.; Clifford, S.; Ochterski, J.; Petersson, G. A.; Ayala, P. Y.; Cui, Q.; Morokuma, K.; Malick, D. K.; Rabuck, A. D.; Raghavachari, K.; Foresman, J. B.; Cioslowski, J.; Ortiz, J. V.; Stefanov, B. B.; Liu, G.; Liashenko, A.; Piskorz, P.; Komaromi, I.; Gomperts, R.; Martin, R. L.; Fox, D. J.; Keith, T.; Al-Laham, M. A.; Peng, C. Y.; Nanayakkara, A.; Gonzalez, C.; Challacombe, M.; Gill, P. M. W.; Johnson, B. G.; Chen, W.; Wong, M. W.; Andres, J. L.; Head-Gordon, M.; Replogle, E. S.; Pople, J. A. *Gaussian 98*, revision A.1; Gaussian, Inc.: Pittsburgh, PA, 1998.

(30) Gmelin, L.; et al. *Gmelins Handbuch Der Anorganishen Chemie*, v. 14.C.1; Verlag Chemie: Leipzig-Berlin, 1970; p 370.

(31) Brocklehurst, B. *Nature* **1968**, *219*, 263. Badger, B.; Brocklehurst, B. *Trans. Faraday Soc.* **1969**, *65*, 2582; *Trans. Faraday Soc.* **1970**, *66*, 2939.

(32) Illies, A. J. *J. Phys. Chem.* **1988**, *92*, 2889. Misev, L.; Illies, A. J.; Jarrold, M. F.; Bowers, M. T. *Chem. Phys.* **1985**, *95*, 469.

(33) Lias, S. G.; Bartmess, J. E.; Liedman, J. F.; Holmes, J. L.; Levin, R. D.; Mallard, W. G. *Gas-Phase Ion Neut. Thermochem., J. Phys. Chem. Ref. Data* **1988**, *17*, Supplement No. 1.

(34) Bowen, K. H.; Eaton, J. G. In *The Structure of Small Molecules and Ions*; Naamna, R., Vagar, Z., Eds.; Plenum: New York, 1987; p 147.

(35) DeLuca, M. J.; Niu, B.; Johnson, M. *J. Chem. Phys.* **1988**, *88*, 5857.

(36) Tsukuda, T.; Johnson, M.; Nagata, T. *Chem. Phys. Lett.* **1997**, *268*, 429.

(37) The $g$ tensor parameters of the $O_3^-$ anion strongly depend on the matrix [see the compilation of EPR parameters in *Landolt-Börnstein Numerical Data and Functional Relationships in Science and Technology*: *Magnetic Properties of Free Radicals*, v. II/9a; Springer-Verlag: New York, 1977; pp 113−116]. The $g$ tensor "matching" of $O_3^-$ in dry ice to $O_3^-$ in anhydrite (with $g_{\|} \approx 2.0102$) given in ref 12 is purely coincidental, as in most matrixes $g_{\|}$ ranges between 2.002 and 2.005.

(38) A very slow endothermic $O^-$ tranfser reaction between $CO_3^-$ and $O_2$ occurs in the gas phase at 200−600 K. See: Dotan, I.; Davidson, J. A.; Streit, G. E.; Albritton, D. L.; Fehsenfeld, F. C. *J. Chem. Phys.* **1977**, *67*, 2874. No such reaction is known to occur in the aqueous solution.

(39) Krishnamurty, M. V. *Mol. Phys.* **1972**, *24*, 1353.

(40) Olsen, J. F.; Burnelle, *J. Am. Chem. Soc.* **1970**, *92*, 3659.

(41) Chantry, G. W.; Horsfield, A.; Morton, J. R.; Whiffen, D. H. *Mol. Phys.* **1962**, *5*, 589. Serway, S. R. A.; Marshall, S. A. *J. Chem. Phys.* **1967**, *46*, 1949.

(42) Eriksson, L. A.; Wang, J.; Boyd, R. J.; Lunell, S. *J. Phys. Chem.* **1994**, *98*, 792. Golding, R. M.; Henchman, M. *J. Chem. Phys.* **1964**, *40*, 1554. Reuveni, A.; Luz, Z. *J. Magn. Reson.* **1976**, *23*, 271.

(43) Eachus, R. S.; Symons, M. C. R. *J. Chem. Soc. A* **1968**, 2438. Taylor, P. C.; Griscom, D. L.; Bray, P. J. *J. Chem. Phys.* **1970**, *54*, 748.

(44) Hunton, D. E.; Albertoni, C. R.; Märk, T. D.; Castleman, A. W., Jr. *Chem. Phys. Lett.* **1984**, *106*, 544. Hiller, J. F.; Vestal, M. L. *J. Chem. Phys.* **1980**, *72*, 4713. Vestal, M. L.; Mauclaire, G. H. *J. Chem. Phys.* **1977**, *67*, 3758. Moseley, J. T.; Cosby, P. C.; Peterson, J. R. *J. Chem. Phys.* **1976**, *65*, 2512

(45) Smith, G. P.; Lee, L. C.; Moseley, J. T. *J. Chem. Phys.* **1979**, *71*, 4034.

(46) Castleman, A. W., Jr.; Hunton, D. E.; Albertoni, C. R.; Hofmann, M.; Lindeman, T. G. *Ber. Bunsen-Ges. Phys. Chem.* **1985**, *89*, 348; *J. Chem. Phys.* **1985**, *82*, 2884 (Note that because of a different choice of the symmetry planes, the $B_2$ representation in the notations of Castleman et al. is equivalent to the $B_1$ representation in the notation adopted in this work, after ref 40 and 41).

(47) Snodgrass, J. T.; Kim, H.-S.; Bowers, M. T. *J. Chem. Phys.* **1988**, *88*, 3072. Roehl, C.; Snodgrass, J. T.; Deakyne, C. A.; Bowers, M. T. *J. Chem. Phys.* **1991**, *94*, 6546.

(48) Hiraoka, K.; Yamabe, S. *J. Chem. Phys.* **1992**, *97*, 643.

(49) Meriaudeau, P.; Vedrine, *J. Chem. Soc., Faraday Trans. 2* **1976**, *72*, 472.

(50) Corcelli, S. A.; Kelley, J. A.; Tully, J. C.; Johnson, M. A. *J. Phys. Chem. A* **2002**, *106*, 4872 and references therein.

(51) The binding energy of water in hexagonal ice is −0.49 eV per molecule; this binding energy is only −0.24 eV for $(H_2O)_2$ [see: Lee, C.; Chen, H.; Fitzgerald, G. *J. Chem. Phys.* **1995**, *102*, 1266 and references therein]. We do not suggest that the energetics of higher $CO_3^-\cdot(H_2O)_n$ clusters can be understood in terms of water−water bonding alone; there should be ion−molecule interactions of the extra water molecules and the $CO_3^-$ core.

(52) Karasawa, H.; Yugeta, R.; Yamaguchi, A.; Sato, S. *Bull. Chem. Soc. Jpn.* **1981**, *54*, 362.